Bipartite magnetic parent phases in the iron oxypnictide superconductor

M. Hiraishi[1], S. Iimura[2], K. M. Kojima[1,3]*, J. Yamaura[4], H. Hiraka[1], K. Ikeda[1], P. Miao[1,3], Y. Ishikawa[1], S. Torii[1], M. Miyazaki[1], I. Yamauchi[1], A. Koda[1,3], K. Ishii[5], M. Yoshida[5,6], J. Mizuki[6], R. Kadono[1,3], R. Kumai[1,3], T. Kamiyama[1,3], T. Otomo[1,3], Y. Murakami[1,3], S. Matsuishi[4] and H. Hosono[2,4]

High-temperature superconductivity appears as a consequence of doping charge carriers into an undoped parent compound exhibiting antiferromagnetic order; therefore, ground-state properties of the parent compound are highly relevant to the superconducting state[1,2]. On the basis of this logic, spin fluctuations have been considered as the origin of pairing of the superconducting electrons in the cuprates[1]. As possible pairing mechanisms, there is growing interest in unconventional spin fluctuations or advanced orbital fluctuations owing to the characteristic multi-orbital states in iron pnictides[3–6]. Here, we report the discovery of an antiferromagnetic phase as well as a unique structural transition in electron-overdoped $LaFeAsO_{1-x}H_x$ ($x \sim 0.5$), whereby a second parent phase is uncovered, albeit heavily doped. The unprecedented two-dome superconducting phases observed in this material can be interpreted as a consequence of the carrier doping starting from the original $x \sim 0$ and additional $x \sim 0.5$ parent phases towards the intermediate region[7]. The bipartite parent phases with distinct physical properties in the second magnetic phase provide us with an interesting example to illustrate the intimate interplay between the magnetic interaction, structural change and orbital degree of freedom in iron pnictide superconductors.

Iron pnictides comprise a new class of high-temperature (high-T_c) superconductors, which has been extensively studied since the discovery of the iron oxypnictide LaFeAsO (La1111; refs 8–14). The superconductivity appears as a result of carrier doping to the parent compound in place of the magnetic- and structural-ordered state[2,9,15]. A recent study reported an advanced doping method using a hydrogen anion instead of fluorine in La1111 that has surpassed the doping limit of fluorine, and uncovered the concealed second superconducting phase (SC2) with a higher T_c of 36 K at $x \sim 0.35$, in addition to the first dome (SC1) with the maximum T_c of 26 K at $x \sim 0.1$ (refs 7,16). To investigate the origin of the two SC domes as well as the origin of the higher T_c in SC2, and to determine whether a certain hidden phase exists beyond the SC2 region, we have performed a multi-probe study in the range $0.40 \le x \le 0.51$ using neutron, muon and X-ray beams.

Figure 1a shows the neutron powder-diffraction pattern in the non-superconducting specimen with $x = 0.51$. Extra peaks were observed with indices $(1/2, 1/2, n)_{T,M}$ ($n = 0, 1, 2$) in the low-temperature region, where the subscripts T and M refer to

the tetragonal cell and magnetic peak, respectively; these were determined to be unambiguously magnetic in origin because they were unobservable in the X-ray measurement. The $(1/2, 1/2, 0)_{T,M}$ reflection gradually gains intensity below the magnetic transition temperature $T_N = 89(1)$ K, estimated by the power law in the $x = 0.51$ sample, as shown in Fig. 1b, which indicates a continuous second-order transition. Similar magnetic peaks were also observed below $T_N \sim 76$ K for $x = 0.45$.

The in-plane magnetic structure is illustrated in the inset of Fig. 1b[17]. The ordering wavevector $\mathbf{q} = (1/2, 1/2, 0)$ was determined to correspond to the magnetic unit cell of $\sqrt{2}\mathbf{a}_T \times \sqrt{2}\mathbf{b}_T \times \mathbf{c}_T$, describing a tetragonal axis, which is consistent with the orthorhombic nuclear unit cell in the low-temperature case. The Fe spins are directed to a diagonal axis of the tetragonal cell, and form an antiferromagnetic collinear structure; this result reveals an exceptional stripe-type arrangement among the iron pnictides[18–21]. The spins couple ferromagnetically along the c axis. The magnetic moment in $x = 0.51$ at 10 K is estimated to be $1.21(1)$ μ_B per iron atom, which is significantly larger than the value of 0.63 μ_B for $x = 0$ (ref. 19). This observation that the long-range magnetic order emerges beyond SC2 is a remarkable finding because the d-electrons on the iron atoms should be delocalized by the large amount of carrier doping and, accordingly, the magnetic interaction is usually expected to be weak.

Figure 2a shows the muon spin relaxation (μSR) time spectra for $x = 0.45$. The slow relaxation above 80 K is attributed to a paramagnetic state, whereas the line shapes below 80 K evolve into strongly damped oscillations with increasing amplitude on cooling, reflecting the development of the magnetically ordered volume fraction (MVF). The significant damping of the muon spin precession in contrast to a clear precession in $x = 0$ (ref. 22) indicates an inhomogeneity in the local magnetic fields, which is presumably due to the heavy doping effect (Supplementary Information).

Figure 2b is a diagram of the μSR process. The amplitude and frequency of the μSR signal reflect the MVF and the ordered moment of the magnetic region, respectively. Figure 2c shows the temperature dependence of the resultant MVF. For $x = 0.51$, the magnetic ordering appears at $T_N = 92(7)$ K and the MVF becomes entire towards zero temperature. As the hydrogen content is reduced, the value of T_N and the MVF decrease in unison. Figure 2d shows the MVF and the superconductivity volume fraction (SVF) estimated from susceptibility measurements[7], clearly indicating an
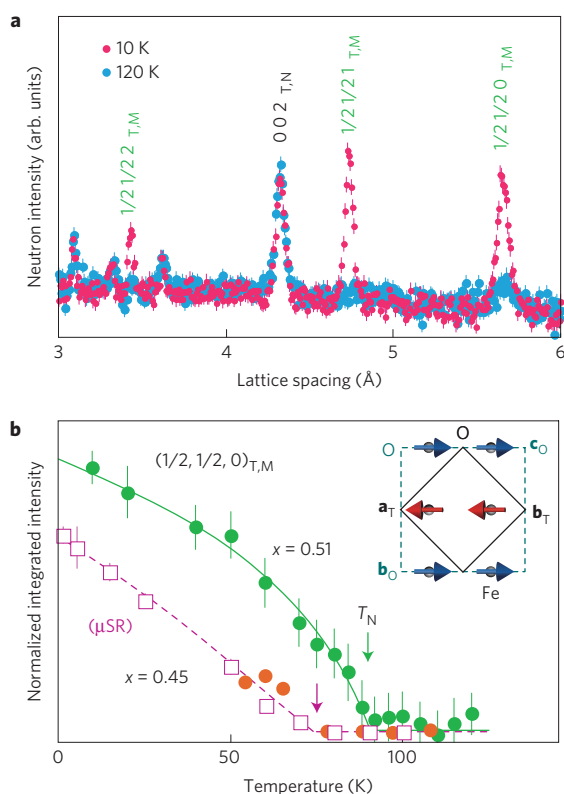
Figure 1 | Pulsed neutron diffraction measurements of LaFeAsO$_{1-x}$H$_x$. We prepared $\sim$1 g powder samples as described in ref. 7 (Supplementary Information). The powder diffraction measurements were performed on the low-angle detector bank of the Super HRPD at J-PARC for $x = 0.51$ and on the NOVA at J-PARC for $x = 0.45$. **a**, Magnetic reflections of $(1/2, 1/2, n)_{T,M}$ ($n = 0, 1, 2$) that were observed clearly at 10 K (for $x = 0.51$) (labelled in green) disappeared at 120 K. **b**, Temperature dependence of the integrated intensity of $(1/2, 1/2, 0)_{T,M}$ in $x = 0.45$ (orange) and 0.51 (green), normalized to the nuclear $(0, 0, 2)_{T,N}$ reflection (labelled in black in Fig. 1a). The data for $x = 0.51$ were fitted to the power law $(T_N - T)^{2\beta}$, resulting in $T_N = 89(1)$ K and $2\beta = 0.58(5)$. The squared order parameter for $x = 0.45$ determined by μSR ($\propto$ (muon frequency)^2 $\times$ (magnetic volume fraction)) is plotted (purple) after scaling to neutron data. The in-plane configuration of the Fe spin, determined by the Rietveld method[17], for $x = 0.45$ as well as 0.51, is illustrated in the inset with the tetragonal unit cell $\mathbf{a}_T \times \mathbf{b}_T$ (solid line) in the high-temperature case and the magnetic unit cell $\sqrt{2}\mathbf{a}_T \times \sqrt{2}\mathbf{b}_T$ (broken line) in the low-temperature case. The error bars represent the statistical error in **a** and the uncertainty in the least-squares fitting of the peaks in **b**.

inverse correlation between the MVF and the SVF. The approximate summation to unity suggests that antiferromagnetic static order and superconductivity coexist in the range $0.40 \leq x \leq 0.45$ despite the absence of the coexistence state in the underdoped region[15]. The coexistence state is not attributed to the microscopic scale but to the mesoscopic scale in the spatial inhomogeneity, because if the coexistence state were due to the microscopic scale the MVF obtained by the μSR experiment would become entire even in the superconducting state (Supplementary Information). Further experimental work will clarify any intimate connection between superconductivity and magnetism in the heavier doping region[23,24].

Figure 3a shows the X-ray profiles of the $(2, 2, 0)_T$ reflections in the $x = 0.45$ and 0.51 samples. On cooling, the peak in the $x = 0.51$ sample was broadened, whereas the peak in $x = 0.45$ exhibited only slight broadening. No broadening of the $(0, 0, l)$ reflections was observed in the $x = 0.51$ sample; therefore, the

experimental findings imply that the tetragonal to orthorhombic (T–O) structural transition emerges clearly for $x = 0.51$.

Figure 3b shows the temperature dependence of the lattice constants in samples with $x = 0.45$ and 0.51. In $x = 0.51$, the a_T axis length splits in two below the T–O transition of $T_s \sim 95$ K, and the c_T axis length shows an upturn at T_s. In $x = 0.45$, although an apparent split between a_T and b_T does not exist, the c_T axis anomaly appears to be similar to that in $x = 0.51$, which may be the result of insufficient coherence of the splitting of a_T and b_T in the low-temperature phase.

The resultant temperature dependence of the structural and magnetic order parameters is shown in Fig. 3c for $x = 0.51$. The small gap between the transition temperatures T_s and T_N implies a strong correlation between structure and magnetism in comparison with the large gap of $\sim$20 K for $x = 0$. On the basis of a structural analysis[25], the compound with $x = 0.51$ crystallizes below T_s in an orthorhombic *Aem*2 structure without inversion symmetry, in contrast to the universal *Cmme* structure with inversion symmetry observed in the 1111 materials (Supplementary Information). The Fe atom exhibits an off-centre deformation in the FeAs$_4$ tetrahedron, as shown in the inset of Fig. 4. The present result provides us with an intriguing deduction that the unusual structural distortion, along with the loss of the inversion symmetry, which has not been found in large ensemble of the iron pnictides[18–21], may profoundly affect the d-orbital levels of the iron atom[26,27].

Figure 4 shows the phase diagram of LaFeAsO$_{1-x}$H$_x$, where the introduction of charge carriers via doping with hydrogen indeed controls the system (Supplementary Information). The features of the physical properties in $x = 0.51$ ($x = 0$) can be characterized as follows: the Fe-spin arrangement is a peculiar stripe-type (universal stripe-type)[18,19]; the magnetic moment is large, 1.21(1) μ_B (small, 0.63 μ_B); the gap between T_s and T_N is $\sim$5 K ($\sim$20 K); the structural symmetry is non-centrosymmetric (centrosymmetric); the magnetic and superconducting states coexist (the magnetic and superconducting states are exclusive) ; the behaviour of resistivity is as for a non-Fermi liquid (Fermi liquid)[7]. These findings strongly suggest the magnetic and electronic correlations are considerably developed in the right-hand region of the phase diagram.

We have thus far regarded the 'undoped' antiferromagnet with the structural transition adjacent to the superconducting state as the parent compound in the high-T_c superconductors. Hence, we now reveal that a newly discovered antiferromagnetic phase with a structural transition adhering to the superconducting phase is considered as the 'doped' parent phase. This behaviour is unexpected, because magnetic and electronic correlations are widely perceived as being weak in the region with heavy carrier doping. However, the magnetic and electronic correlations in the advanced parent phase at $x \sim 0.5$ are indeed rather strong in comparison to the original parent phase at $x \sim 0$. We think that a multi-band feature such as an orbitally selective Hund's coupling or a Mott transition plays a crucial role so as to drive the emergence of the advanced parent phase, which is presumably stimulated by the half-integer number of the $d^{6.5}$ state in $x = 0.5$ (refs 28,29). In the iron pnictides, the 'parent compound' not only refers to the undoped material, but also more generally indicates a fingerprint at a certain critical point of the magnetic and electronic correlations. Yamakawa *et al.* proposed spin and orbital ordered states with the commensurate Fermi surface nesting at $x = 0$ and the incommensurate Fermi surface nesting at $x \sim 0.4$ in LaFeAsO$_{1-x}$H$_x$ from the theoretical calculation[30]; the latter inconsistency with the present result is presumably due to the sizeable electron correlation with the large magnetic ordered moment. A more sophisticated theory concerning the electron correlation, the multi-band picture, and the heavy doping effect in the crystal is required to specify the origin of the advanced parent phase.

We now discuss the origin of the two-dome SC phases. The electron doping to the d^6 state of the $x = 0$ parent—that is, the
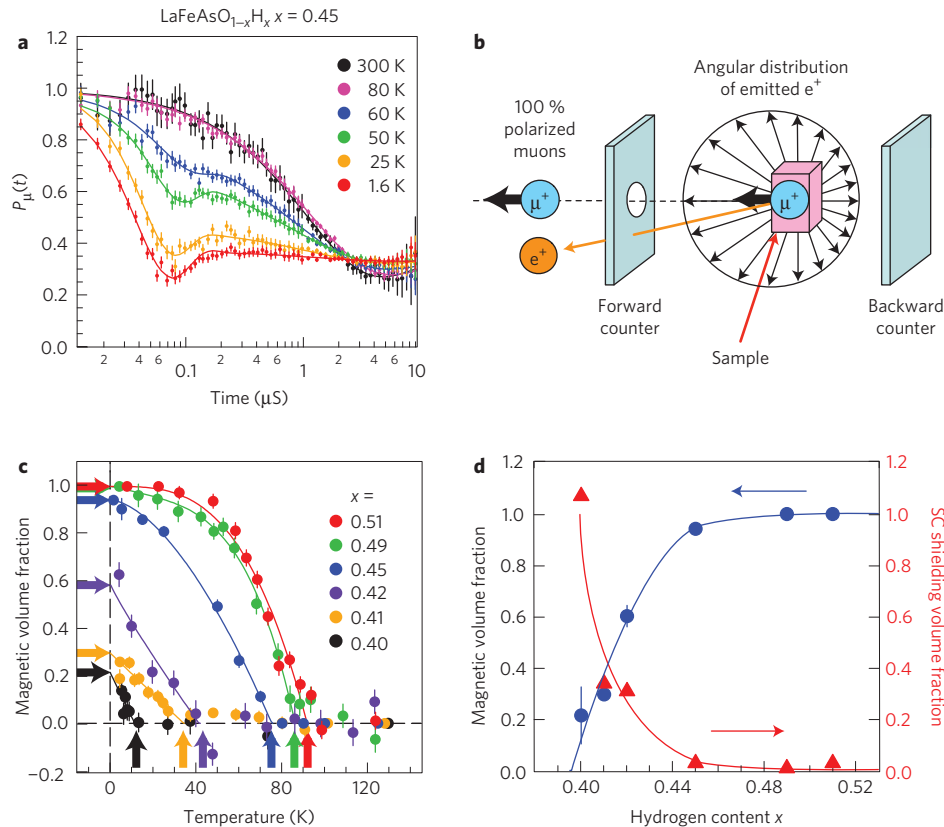
Figure 2 | Zero-field muon spin relaxation measurements. a, Time spectra of the muon polarization P_μ for $x = 0.45$, taken at PSI. The data exhibit significant damping in contrast to a clear muon spin precession in $x = 0$ (ref. 22), indicating an inhomogeneity in the local magnetic fields. **b**, Diagram of the muon spin relaxation process. The magnetic volume fraction (MVF) is estimated from the amplitude of the time-dependent asymmetry in the positron counts between the forward and backward counters. **c**, Temperature dependence of the MVF for samples in the range $x = 0.40 - 0.51$, conducted at J-PARC MUSE and PSI. **d**, Hydrogen concentration dependence of the MVF (blue) and the superconductivity (SC) shielding volume fraction (red). The error bars represent the statistical error in **a** and the uncertainty in the least-squares fittings of the spectra in **c** and **d**.
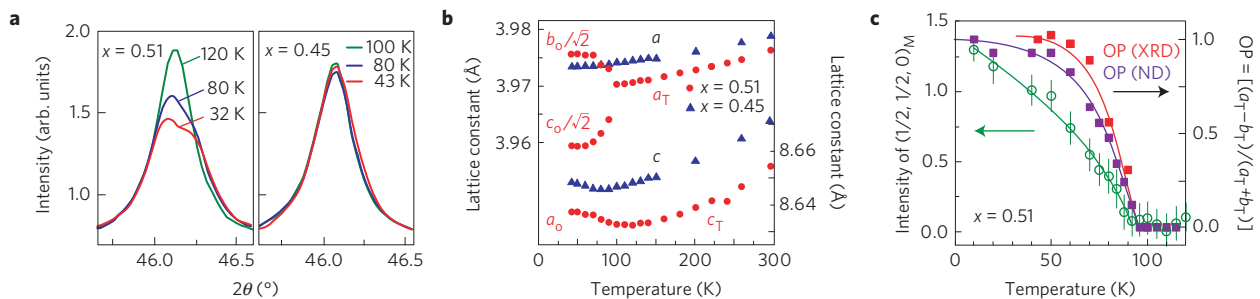

Figure 3 | Synchrotron X-ray diffraction measurements. Powder diffraction measurements for samples with $x = 0.42, 0.45, 0.49$ and 0.51 were performed on the beamlines of 8A/8B at KEK-PF. **a**, Representative profiles of the $(2, 2, 0)_T$ reflections for $x = 0.45$ and 0.51 at a wavelength of $\lambda = 1.0993$ Å. Peak broadening was observed in $x = 0.51$ below $T_s \sim 95$ K, whereas there was slight broadening in $x = 0.45$. **b**, The temperature dependence of the lattice constants for $x = 0.45$ and 0.51. In $x = 0.51$, the a_T- and c_T-axes exhibit a split in length and an upturn with the T–O transition of $T_s \sim 95$ K, respectively. In the orthorhombic phase, the values of b_O and c_O are divided by $\sqrt{2}$. The cell setting changes as $\mathbf{a}_O = \mathbf{c}_T$, $\mathbf{b}_O = \mathbf{a}_T + \mathbf{b}_T$ and $\mathbf{c}_O = -\mathbf{a}_T + \mathbf{b}_T$ (Fig. 1b inset). The orthorhombicity, $\Delta a_T/a_T = 0.41\%$, is smaller than that of the other iron pnictides (0.49%, LaFeAsO; 0.73%, $BaFe_2As_2$; refs 18,20). **c**, Temperature dependence of the structural order parameter (OP) determined by neutron and X-ray diffraction, and the magnetic intensity of the $(1/2, 1/2, 0)_{T,M}$ reflection in $x = 0.51$. The error bars indicate the uncertainty in the least-squares fitting of the magnetic peaks in **c**.

chemical substitution of H^- to the O^{2-} site—leads to the SC1 phase. From the viewpoint of the $x \sim 0.5$ parent, the SC2 phase emerges through hole doping to the $d^{6.5}$ state, by O^{2-} substitution to the H^- site. Consequently, we can definitely state that the two SC domes are generated by carrier doping, starting from the left- and right-hand parent compounds towards the intermediate region of the phase diagram. Moreover, the T_c valley at $x \sim 0.2$ is interpreted as a unique crossover region in this phase diagram.

The combination of the distinct feature of the structural instability with the loss of inversion symmetry and the localized nature of the d-electrons relative to the original parent compound plausibly result in a new mechanism of superconductivity as the origin of the significant enhancement of T_c in SC2 relative to SC1, because the ground-state properties in the parent compounds generally persist unabated, even in the superconducting state. Future band structure calculations taking into account the orthorhombic
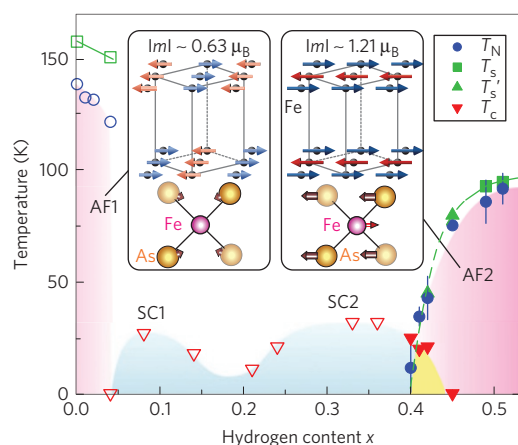
Figure 4 | Magnetic, structural and superconducting phase diagram of LaFeAsO₁₋ₓHₓ. The original parent compound with $x = 0$ exhibits a structural transition at $T_s = 155$ K, followed by an antiferromagnetic state (AF1) at $T_N = 137$ K (ref. 18). With increasing x, two superconductivity domes appear: $0.05 \leq x \leq 0.20$ (SC1) with $T_{c,max} = 26$ K, and $0.20 \leq x \leq 0.42$ (SC2) with $T_{c,max} = 36$ K (ref. 7). Eventually, another antiferromagnetic phase (AF2) appears in the range $0.40 \leq x \leq 0.51$. In the advanced parent compound at $x = 0.51$, structural and magnetic transitions occur at $T_s \sim 95$ K and $T_N = 89$ K, respectively. T_s' indicates the c axis upturn temperature observed in X-ray measurements. The filled and open marks are obtained from the present and previous results, respectively[7]. The magnetic structures of AF1 (left) and AF2 (right) are shown with their magnetic moments m (ref. 19), where the solid lines represent the tetragonal cell. The displacements of the Fe and As atoms across the structural transitions are schematically described by the arrows on the FeAs₄ tetrahedra from the view of the orthorhombic long axis, in which the Fe and As atoms move by 0.07 Å (0 Å) and 0.06 Å (0.01 Å) in $x = 0.51$ ($x = 0$), respectively. The error bars represent the uncertainty in the least-squares fitting routines.

crystal and magnetic structures would confirm and clarify this new ordered state.

References

1. Lee, A. P., Nagaosa, N & Wen, X-G. Doping a Mott insulator: Physics of high-temperature superconductivity. *Rev. Mod. Phys.* **78**, 17–85 (2006).
2. Paglione, J. & Greene, R. L. High-temperature superconductivity in iron-based materials. *Nature Phys.* **6**, 645–658 (2010).
3. Singh, D. J. & Du, M-H. Density functional study of LaFeAsO₁₋ₓFₓ: A low carrier density superconductor near itinerant magnetism. *Phys. Rev. Lett.* **100**, 237003 (2008).
4. Kuroki, K. *et al.* Unconventional pairing originating from disconnected Fermi surfaces of superconducting LaFeAsO₁₋ₓFₓ. *Phys. Rev. Lett.* **101**, 087004 (2008).
5. Mazin, I., Singh, D. J., Johannes, M. D. & Du, M. H. Unconventional superconductivity with a sign reversal in the order parameter of LaFeAsO₁₋ₓFₓ. *Phys. Rev. Lett.* **101**, 057003 (2008).
6. Kontani, H. & Onari, S. Orbital-fluctuation-mediated superconductivity in iron pnictides: Analysis of the five-orbital Hubbard–Holstein model. *Phys. Rev. Lett.* **104**, 157001 (2010).
7. Iimura, S. *et al.* Two-dome structure in electron-doped iron arsenide superconductors. *Nature Commun.* **3**, 943 (2012).
8. Kamihara, Y. *et al.* Iron-based layered superconductor: LaOFeP. *J. Am. Chem. Soc.* **128**, 10012–10013 (2006).
9. Kamihara, Y., Watanabe, T., Hirano, M. & Hosono, H. Iron-based layered superconductor La[O₁₋ₓFₓ]FeAs ($x = 0.05 - 0.12$) with $T_c = 26$ K. *J. Am. Chem. Soc.* **130**, 3296–3297 (2008).

10. Chen, X. H. *et al.* Superconductivity at 43 K in SmFeAsO₁₋ₓFₓ. *Nature* **453**, 761–762 (2008).
11. Takahashi, H. *et al.* Superconductivity at 43 K in an iron-based layered compound LaO₁₋ₓFₓFeAs. *Nature* **453**, 376–378 (2008).
12. Rotter, M., Tegel, M. & Johrendt, D. Superconductivity at 38 K in the iron arsenide (Ba₁₋ₓKₓ)Fe₂As₂. *Phys. Rev. Lett* **101**, 107006 (2008).
13. Yildirim, T. Origin of the 150-K anomaly in LaFeAsO: Competing antiferromagnetic interactions, frustration, and a structural phase transition. *Phys. Rev. Lett.* **101**, 057010 (2008).
14. Ma, F. & Lu, Z-Y. Iron-based layered compound LaFeAsO is an antiferromagnetic semimetal. *Phys. Rev. B* **78**, 033111 (2008).
15. Luetkens, H. *et al.* The electronic phase diagram of the LaO₁₋ₓFₓFeAs superconductor. *Nature Mater.* **8**, 305–309 (2009).
16. Matsuishi, S. *et al.* Structural analysis and superconductivity of CeFeAsO₁₋ₓHₓ. *Phys. Rev. B* **85**, 014514 (2012).
17. Rodriguez-Carvajal, J. Recent advances in magnetic structure determination by neutron powder diffraction. *Physica B* **192**, 55–69 (1993).
18. De la Cruz, C. *et al.* Magnetic order close to superconductivity in the iron-based layered LaO₁₋ₓFₓFeAs systems. *Nature* **453**, 899–902 (2008).
19. Qureshi, N. *et al.* Crystal and magnetic structure of the oxypnictide superconductor LaFeAsO₁₋ₓFₓ: A neutron-diffraction study. *Phys. Rev. B* **82**, 184521 (2010).
20. Huang, Q. *et al.* Neutron-diffraction measurements of magnetic order and a structural transition in the parent BaFe₂As₂ compound of FeAs-based high-temperature superconductors. *Phys. Rev. Lett.* **101**, 257003 (2008).
21. Lumsden, M. D. & Christianson, A. D. Magnetism in Fe-based superconductors. *J. Phys. Condens. Matter* **22**, 203203 (2010).
22. Klauss, H-H. *et al.* Commensurate spin density wave in LaFeAsO: A local probe study. *Phys. Rev. Lett.* **101**, 077005 (2008).
23. Uemura, Y. J. Superconductivity: Commonalities in phase and mode. *Nature Mater.* **8**, 253–255 (2009).
24. Takeshita, S. *et al.* Insular superconductivity in a Co-doped iron pnictide CaFe₁₋ₓCoₓAsF. *Phys. Rev. Lett.* **103**, 027002 (2009).
25. Izumi, F. & Momma, K. Three-dimensional visualization in powder diffraction. *Solid State Phenom.* **130**, 15–20 (2007).
26. Lee, C-C., Yin, W-G. & Ku, W. Ferro-orbital order and strong magnetic anisotropy in the parent compounds of iron-pnictide superconductors. *Phys. Rev. Lett.* **103**, 267001 (2009).
27. Lv, W., Wu, J. & Phillips., P. Orbital ordering induces structural phase transition and the resistivity anomaly in iron pnictides. *Phys. Rev. B* **80**, 224506 (2009).
28. de' Medici, L., Hassan, S. R., Capone, M. & Dai, X. Orbital-selective Mott transition out of band degeneracy lifting. *Phys. Rev. Lett.* **102**, 126401 (2009).
29. Lanatà, N. *et al.* Orbital selectivity in Hund's metals: The iron chalcogenides. *Phys. Rev. B* **87**, 045122 (2013).
30. Yamakawa, Y. *et al.* Phase diagram and superconducting states in LaFeAsO₁₋ₓHₓ based on the multiorbital extended Hubbard model. *Phys. Rev. B* **88**, 041106(R) (2013).

Author contributions

Y.M., R. Kadono, S.I., S.M. and H. Hosono conceived the study. M.H., K.K., M.M., I.Y., A.K. and R. Kadono carried out the muon experiment. S.I. synthesized the samples. J.Y. and R. Kumai measured the synchrotron X-ray diffraction. H. Hiraka, J.Y., K. Ikeda, P.M., Y.I., S.T., T.K. and T.O. performed the neutron scattering experiments. J.Y., M.Y. and K. Ishii measured the X-ray absorption. M.H., K.K., J.Y. and H. Hiraka co-wrote the manuscript. All the authors discussed the results and the manuscript.

Additional information

Supplementary information is available in the online version of the paper. Reprints and permissions information is available online at www.nature.com/reprints. Correspondence and requests for materials should be addressed to K.K.

Competing financial interests

The authors declare no competing financial interests.